Cement and Concrete Research 201 (2026) 108125

Contents lists available at ScienceDirect

Cement and Concrete Research

journal homepage: www.elsevier.com/locate/cemconres

^{1}H NMR relaxation analysis of cement-based materials: The spin-lock $T_{1\rho}$ experiment and the partitioning of water in C-S-H inter-layer spaces☆,☆☆

Peter J. McDonald [a,b,*], David A. Faux [b], Longfei Ma [a], Hong Wong [a]

[a] Imperial College London, Department of Civil and Environmental Engineering, London, SW7 2AZ, UK
[b] University of Surrey, School of Mathematics and Physics, Guildford, GU2 7XH, UK

ARTICLE INFO

Keywords:
C-S-H
Cement
Porosity
^{1}H NMR
Water

ABSTRACT

In recent years,^{1}H NMR relaxometry has become a mainstream methodology for study of the nano-porosity of cement-based materials. For the most part, measurements have been carried out using variants of the classic CPMG T_2 and solid-echo NMR pulse sequences and, to a lesser extent, the inversion recovery T_1 sequence.

Notwithstanding considerable successes, these methods all have one or another disadvantage, quite often associated with reliable differentiation of the so-called inter-layer and quasi-crystalline water fractions. In this paper, we introduce the application of the $T_{1\rho}$ spin-lock experiment as a convenient alternative methodology. Early results are presented. Measuring $T_{1\rho}$ overcomes some of the earlier difficulties, potentially has some wider advantages but also has raised some interesting questions of interpretation associated with the partitioning of water between C-S-H interlayer spaces and quasi-crystalline phases.

1. Introduction

It is now 15 years since one of us (PJM) spent a year working with Karen Scrivener at EPFL. That year led to two papers [1,2] that demonstrated the use of ^{1}H NMR relaxometry to the measurement of the growth and densification of C-S-H during hydration and to the measurement of the pore size resolved cement sorption isotherm. While not the first demonstration of ^{1}H NMR in cements, that honour goes to Robert Blinc [3], and notwithstanding important contributions from the Pintar/Peemoeller group [4], these were the first papers to gain wider acceptance for the method from, at that time, a somewhat sceptical cement science audience. Since the early 2000s, our group has demonstrated *inter-alia* the effects of temperature [5] and additives [6] on the pore size distribution during hydration. We have evidenced water exchange between pores and spaces of different size [7,8] in saturated material. We have shown that water distribution within the porosity of cement changes in response to temperature [9] and pressure [10] and that the pore size distribution itself is dynamic and relaxes in response to sudden changes in saturation [11,12] and shown how this can be seen as one cause (likely amongst others) of anomalous water sorption [13] with a pronounced sample size effect [14]. The experimental work has been accompanied by lattice Boltzmann modelling of the dynamics [15,16], Monte Carlo modelling of microstructure growth [17] and of NMR relaxation in nanoscale pores [18,19]. Highlights of this work from the global COVID-19 pandemic era, especially as it concerns dynamic porosity, were reviewed in the LCCS presentation linked to this paper. Reviews have also been published [20,21] as have practical guides to the methodology specific to cement [22,23]. The presentation went on to introduce new work, specifically the introduction of the spin-lock $T_{1\rho}$ experiment [24] to the analysis of cements. $T_{1\rho}$ has previously been applied to the study of oil and water in reservoir rocks [25]. It has found wider application, and been more broadly developed, in bio-medical applications [26]. The new application to cement is described more fully in the remainder of this paper.

2. NMR pulse sequences

The experiments reported above have, almost without exception, been carried out using variations of three basic NMR pulses sequences: CPMG standing for Carr–Purcell–Meiboom–Gill sequence [27] to measure the NMR spin–spin relaxation time T_2; the solid echo sequence [28] sometimes dubbed 'quad echo' to measure the crystalline solid to evaporable water fractionation; and the solid-echo extension, the quadrature echo train that finds particular use in strong gradient magnetic fields

☆ This article is part of a Special issue entitled: 'Low-carbon cement science' published in Cement and Concrete Research.

☆☆ The full results introduced in this paper were outlined at LCCS 2005 under the title: '^{1}H NMR Relaxation Analysis of cements: looking backwards, looking forwards'.

* Corresponding author at: Imperial College London, Department of Civil and Environmental Engineering, London, SW7 2AZ, UK.
E-mail address: peter.mcdonald@imperial.ac.uk (P.J. McDonald).

https://doi.org/10.1016/j.cemconres.2025.108125
Received 11 July 2025; Received in revised form 29 October 2025; Accepted 16 December 2025
Available online 23 December 2025

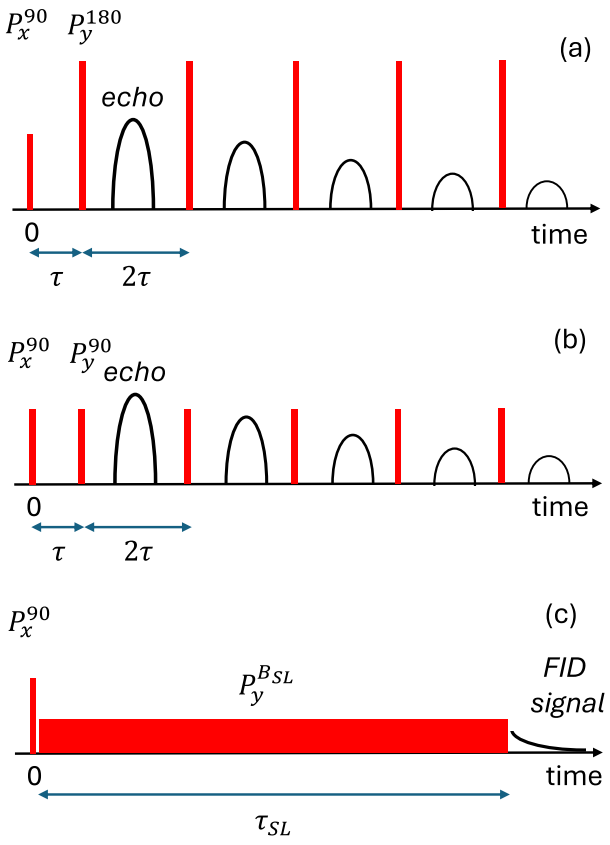

Fig. 1. NMR pulse sequences. (a) CPMG used to measure T_2 and hence evaporable water fractionation by pore size. (b) Quadrature echo train measures a poorly defined relaxation time between T_2 and $T_{1\rho}$. Reduced to just the first echo with short τ, it is the solid (sometimes called 'quad') echo sequence used to measure the solid/mobile water fractionation. (c) Spin-lock sequence to measure $T_{1\rho}$.

e.g. as used for imaging cements [29]. Alternate to the T_2 relaxation time, others have used the spin-lattice relaxation time, T_1 as measured using an inversion recovery sequence [30,31].

2.1. CPMG

The CPMG NMR pulse sequence, Fig. 1a comprises, in standard notation:

$$P_x^{90} - \tau - (P_y^{180} - 2\tau)_n.$$

An NMR echo forms at the centre of each 2τ window. The resultant n-echo train comprises multiple exponential decay components each of amplitude directly proportional to the mass density of mobile water in a characteristic pore size in the sample, such as gel-pore water. The components are distinguished by differing T_2 relaxation decay times. For practical reasons the minimum echo time is typically of the order of 50-60 μs. The primary reason is that, if it is too much smaller, then the first echo is corrupted by residual signal from water (strictly ^{1}H) chemically combined into crystalline and quasi-crystalline environments such as portlandite and ettringite. If it is longer, then the inter-layer water is missed.

2.2. Inversion recovery

The inversion recovery experiment is written:

$$P_x^{180} - \tau_{inv} - P_x^{90}.$$

The intensity of the free induction decay signal immediately following the P_x^{90} pulse is recorded as a function of τ_{inv}. Like T_2, T_1 varies with pore size. The primary advantage of T_1 compared to T_2 is that the magnetisation recovery is unaffected by water diffusion in the susceptibility magnetic field gradients of small pores. The disadvantages are that the experiment requires more time and the exponential fitting of magnetisation *recovery* curves requires good knowledge of the equilibrium value. A small equilibrium measurement error seriously impacts the fitting. In the case of T_2 *decay*, the equilibrium is unequivocally 0.

2.3. Solid echo

In standard notation the solid echo sequence is written:

$$P_x^{90} - \tau - P_y^{90} - \tau.$$

This sequence refocuses magnetic dipolar interaction broadening of 'stationary' nuclei and so prolongs the apparent T_2 of the (quasi-) crystalline ^{1}H. Thus a 'solid' echo forms at time 2τ. The minimum echo time is normally dictated by the pulse lengths and the instrument dead time: typically $2\tau = 24$ μs for our equipment. The solid echo is superimposed on an exponential decay for mobile ^{1}H (evaporable water). Both are measured as a function of τ typically in the range 12–50 μs. The τ dependent intensities are back-extrapolated to zero τ in order to estimate the solid mass fraction of ^{1}H. Gaussian curves are usually employed both to fit individual echoes (to measure the intensities) and to back extrapolate their intensities. This second Gaussian analysis is problematic: it can under estimate the echo intensity. The alternate option is an exponential decay back extrapolation although this is generally worse in the other direction. The exact τ dependence is a complex function of molecular/crystal structure and is generally unknown.

2.4. Quadrature echo train

The quadrature echo train, Fig. 1b, is an extension of the solid echo:

$$P_x^{90} - \tau - (P_y^{90} - 2\tau)_n$$

This experiment has the advantage needed in strong magnetic field gradients of optimising for short pulses of constant high bandwidth. Echoes are measured in the middle of each 2τ window just like CPMG except that the intensity of the first few echoes (in a gradient field) is strongly modulated. The modulation is removed either by application of theory or, more commonly calibration with a standard sample. The measured decay constant is a hybrid of T_2 and $T_{1\rho}$ where the latter is the T_1 relaxation time measured in what NMR spectroscopists call the rotating reference frame, a reference frame that precesses at the NMR frequency around the static magnetic field, B_0. As the pulse gap is made smaller, so the decay is weighted more and more towards $T_{1\rho}$, away from T_2.

The question arises: what if the pulse gap is reduced to zero?

3. Spin-lock $T_{1\rho}$ experiment

The quadrature echo train with the pulse gap reduced to zero is the classic $T_{1\rho}$ spin-lock experiment [24], Fig. 1c, written as

$$P_x^{90} P_y^{B_{SL}}(\tau_{SL})$$

Here $P_y^{B_{SL}}(\tau_{SL})$ is a spin-lock pulse of amplitude B_{SL}, duration τ_{SL} and phase y. Of course, now there are no echoes. Rather the magnetisation is measured in the form of a free induction decay (FID) after the long duration spin-lock pulse. The experiment is repeated multiple times for multiple τ_{SL}.

The spin lock pulse 'fixes' or 'locks' the orientation of the magnetisation in the rotating reference frame in the direction of B_{SL} and will be familiar to high field spectroscopists as part of a double-resonance cross-polarisation experiment. The $T_{1\rho}$ time is the characteristic decay

time for this 'fixation'. Thus the intensity of the measured FID is found to decrease exponentially with characteristic time $T_{1\rho}$ as τ_{SL} is increased. A simple way to interpret $T_{1\rho}$ is to recognise it as the T_1 time that would normally be measured if the static magnetic field were extremely small, the strength of B_{SL} rather than B_0. B_{SL} is typically 1000 times less than B_0.

The overall experiment duration is closer in length to measuring T_1 with inversion recovery (say 10–20 min) compared to T_2 with CPMG (say 1 min) for a reasonable number of averages. However, it has several advantages to compensate.

First, the spin-lock pulse can be made short, and incremented in steps short, compared to the 2τ of CPMG. Therefore, the first advantage is that more data points encapsulating the early decay of (especially) the inter-layer water can be recorded. This advantage significantly aides data fitting.

Second, the $T_{1\rho}$ of mobile water ^{1}H may be longer (and certainly no shorter) than T_2. A longer $T_{1\rho}$ (compared to T_2) facilitates data fitting even more.

Third, $T_{1\rho}$, like high field T_1, is unaffected by water diffusion in magnetic susceptibility gradients occasioned by small pores and paramagnetic ions. This, and the potentially longer relaxation time compared to T_2, should enable easier working with, for instance, grey cements with greater paramagnetic ion densities although this has not yet been tested.

A fourth advantage is the one that encouraged us to towards this experiment in the first place, although results here are not yet presented. In the late 1990's/early 2000's, Korb and co-workers [32,33] advocated the use of NMR field cycling methods to measure the very low frequency dependence of NMR relaxation times for water in C-S-H pores. Undoubtedly the information content at, and as a function of, ultra-low frequency (kHz) is very rich. Recent theoretical approaches to understanding water dynamics in small pores at low frequency by one of us (DAF) [18,19,34] and the recent availability of software to perform the complex integrations required for numerical data fitting [35] suggest it should be strongly pursued with renewed vigour. However, the field cycling experiment requires very specialist equipment. The authors are aware of about 15 field-cycling instruments across Europe. However, only a sub-set are suitable for cement-materials work and, for that purpose, we have collaborated with the groups in Bologna [19], Dublin [36] and Cluj [37]. There is similar paucity of suitable instrumentation in North America and elsewhere. Also the field cycling experiment is severely limited as to the shortest relaxation time that can be measured, a few milliseconds compared to hundreds of microseconds as ideally wanted. Moreover, it measures only a proxy for the relaxation time, not the relaxation time *per-se* without considerable experimental complexity and overall increase in measurement time. Consequently, field cycling is unsuited to hydrating cements beyond the first (typically) 8-12 h; around the end of a typical induction period. By measuring $T_{1\rho}$ as a function of the spin-lock pulse *intensity* these restrictions are largely overcome and we expect to report examples in the near future.

4. Methods and materials

White cement powder similar to that which we have previously used [13] was mixed in small quantities (8 g) with water to make a paste of water to cement ratio by mass of 0.4 using procedures very largely akin to those we have previously described: specifically 2 min mixing with a Vortex mixer. Small aliquots of paste (typically about 1 cc) were syringed into 10 mm NMR tubes. The tubes were sealed and allowed to cure at room temperature with periodic NMR measurements.

Experiments were carried out using a Magritek KEA^2 NMR spectrometer operating at 20 MHz. The P^{90} and P^{180} pulse lengths were both 5 μs.

For CPMG and quadrature echo trains, 256 linearly spaced echoes were acquired with a pulse gap of τ = 30 μs (echoes spaced every 2τ = 60 μs).

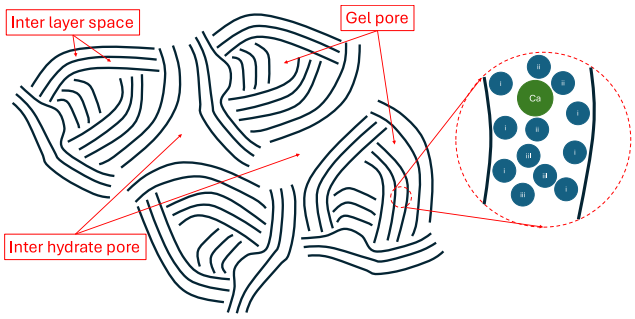

Fig. 2. Main plot: The lines are hydrate backbone layers separated by *c.* 1 nm. They define water filled inter-layer spaces, gel pores and inter-hydrate pores. Largely self-dessicated capillary shrinkage pores are on a much larger scale and are not shown. Expanded region: The inter-layer space has (i) OH associated with surface sites; (ii) water associated with calcium ions and (iii) less constrained water.

For solid measurement a single quadrature echo and background free induction decay signal were recorded for the set of τ values 12, 15, 19, 24, 30, 37, 45, 54 μs.

For $T_{1\rho}$ experiments a standard P^{90} pulse was applied followed immediately by a long duration spin-lock pulse, its amplitude reduced by −17 dB equating to a spin-lock frequency of 7 kHz. This low value was chosen to protect the probe from burn out during these early measurements. The FID amplitude was measured 20 μs after the end of the long pulse. Measurements were made for 50 long pulse durations approximately logarithmically spaced in the range 18 to 5000 μs.

In CPMG, quadrature echo train and $T_{1\rho}$ experiments 128, 128 and 16 averages respectively were acquired. In all experiments, a repetition time of 1.5 s was used.

Data was acquired quasi-continuously for more than 1 month of hydration using solid echo, quadrature echo train and spin-lock $T_{1\rho}$. Occasional CPMG sequences were recorded as was the signal from a standard dilute solution of $MnCl_2$. All cement data was normalised to the signal intensity recorded from the standard.

Multicomponent exponential decays (each of CPMG, quadrature echo train and $T_{1\rho}$ yield a decay signal) were fit using a combination of least squares and exponential stripping methods as previously described. 4 component fits were attempted with the components representing inter-layer, gel, inter-hydrate and capillary space/pore water, shown schematically in Fig. 2. For CPMG the first three T_2 values were constrained in the ratios 1:3:12 broadly in accord with previous work where we have variously used 1:3:9, 1:4:16 and 1:3.5:3.5^2. The capillary water T_2 is very much longer and was allowed, along with the amplitudes, to float. For the quadrature echo train and $T_{1\rho}$ experiments the constraints are discussed below.

For solid echo, the signal was fit to a Gaussian echo and single component (T_2^*) exponential decay as previously described. The intensities as a function of τ were back extrapolated to zero τ to infer the fraction of total water incorporated in quasi-crystalline solids.

5. Results and analysis

In general, data related to CPMG/solid echo is coloured green; quadrature echo train blue and spin-lock $T_{1\rho}$ red.

5.1. CPMG and quadrature echo measurements at day 39

Fig. 3 shows the CPMG decay of a w/c = 0.4 paste at day 39. The decay, shown on a log–log plot is fit to a 4-component exponential decay representing C-S-H inter-layer, gel, inter-hydrate and capillary pore water. The T_2 values are 0.1, 0.3, 1.2 and 50 ms respectively, in general accord with our previous work. The quasi crystalline solid

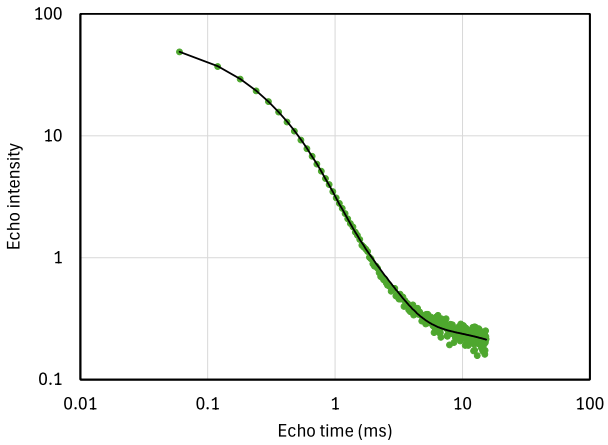

Fig. 3. CPMG decay data and fit for the paste at day 39.

'water' and total mobile water fractions were calculated by back extrapolation of signals from the quadrature echo experiment, again as previously described, Fig. 4. The same ratios were also determined from the CPMG signal loss compared to the freshly mixed paste. The resultant amplitude fractions are shown as green bars in Fig. 5. Here the capillary fraction is combined with the inter-hydrate fraction for simplicity. For a mature paste the former is always very small since the large capillary pores self-dessicate. The amplitudes are compared with average values taken from Muller et al. [1,2] (grey bars) which we regard as a bench-mark results for this type of cement. The agreement is generally very good first between the bench-mark and new results and between the two ways in which the solid fraction has been measured.

5.2. Quadrature echo train at day 39

Fig. 6 shows an overlay of the CPMG and quadrature echo train data. The later was measured exactly as the former, except that the refocussing pulse amplitudes were reduced from P^{180} to P^{90}. The overlay is good except that the first few quadrature echo points slightly exceed their CPMG counterparts. The quadrature echo train data has been fit to a 4 component exponential decay using the same T_2 relaxation times as for CPMG. The resultant amplitudes are shown as blue bars in Fig. 5, confirming that the inter-layer signal is a little enhanced. The solid fraction, which is measured from the signal loss compared to day zero is correspondingly reduced.

The explanation is as follows. The formation of the first echo of this sequence is identical to the formation of a quadrature echo with a large pulse gap and so the incorporation of a certain amount of quasi-crystalline solid signal is to be expected. This carries through for the first few echoes of the quadrature echo train. Thus the CPMG and quadrature echo sequence data overlay each other to a good approximation except for this early enhancement. Indeed, simplistically arguing that if the solid echo intensity recorded at 60 μs is back extrapolated to zero time using an exponential with time constant 100 μs as for the inter-layer, then the solid fraction is underestimated by a little *over* half, not so far from the little *under* half actually observed.

5.3. Spin-lock $T_{1\rho}$ at day 39

Comparable to Fig. 6, Fig. 7 shows spin-lock $T_{1\rho}$ data and fit overlain on CPMG data at day 39. This time, it is seen that the inter-layer signal represented by the early data points is *diminished* compared to CPMG. The fit component amplitudes using $T_{1\rho}$ relaxation times equal to the corresponding T_2 times are shown as red bars in Fig. 5. The quasi crystalline solid is about 50% larger than the bench mark and

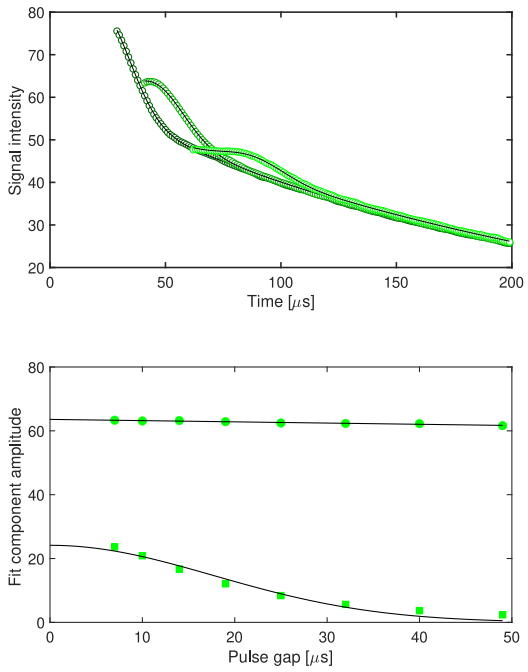

Fig. 4. Upper plot: Quadrature echo data (symbols) and total fits (lines) using a Gaussian (for solid) and exponential (for mobile) decay components all overlain for τ = 12 (dark green), 24 (mid green) and 45 μs (light green). As expected, the data sets overlay each other beyond the echoes that appear at 2τ. Lower plot: The Gaussian and exponential fit amplitudes for all pulse gaps (τ−5 μs) with Gaussian and exponential fits from which the quasi solid and mobile intensities are determined to be 24.1 and 63.6 so 27 and 83% respectively. (For interpretation of the references to colour in this figure legend, the reader is referred to the web version of this article.)

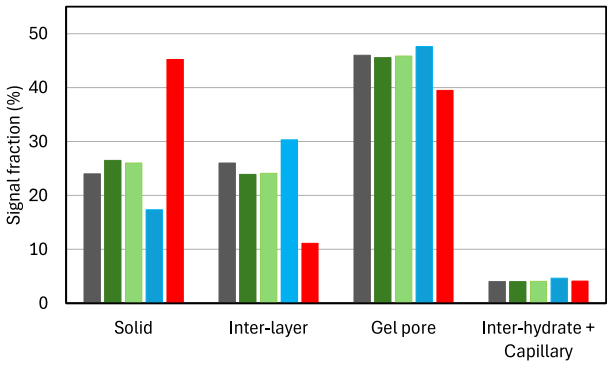

Fig. 5. Water fractionation for the 39-day paste. Grey bars are benchmark results averaged from Muller et al. [1,2]. Dark and light green bars are calculated from the CPMG and solid echo experiments (as usual) and entirely from CPMG (signal loss) respectively. Blue bars are calculated from quadrature echo train and signal loss. Red bars are from spin-lock $T_{1\rho}$ and signal loss. (For interpretation of the references to colour in this figure legend, the reader is referred to the web version of this article.)

the inter-layer signal correspondingly smaller. There is a similar but proportionately smaller effect taking place in the gel signal.

This highly repeatable result is a surprise. It is both larger, and opposite to, that seen with quadrature echo train. The same explanation cannot therefore apply. It is discussed further in Section 6. First however, and to emphasise the point, Fig. 8 shows the signal fractions recorded for the $T_{1\rho}$ experiment as a function of time. It broadly looks like Fig. 2 in Muller et al. 2013 [1] except that the solid fraction is very much larger and the inter-layer much smaller than before.

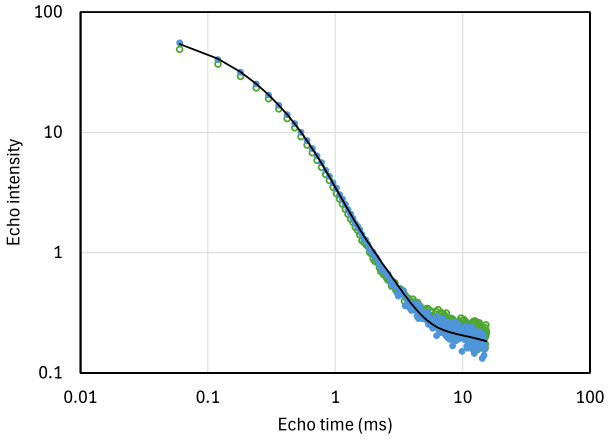

Fig. 6. Quadrature echo train data (blue solid symbols) and data fit (solid line) overlain on CPMG data (open green symbols). (For interpretation of the references to colour in this figure legend, the reader is referred to the web version of this article.)

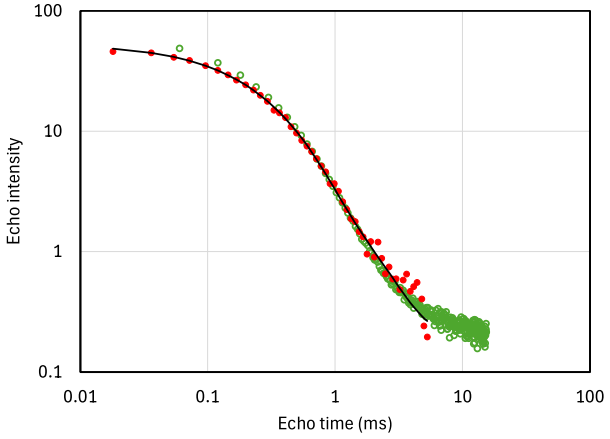

Fig. 7. $T_{1\rho}$ data (red solid symbols) and data fit (solid line) overlain on CPMG data (open green symbols). (For interpretation of the references to colour in this figure legend, the reader is referred to the web version of this article.)

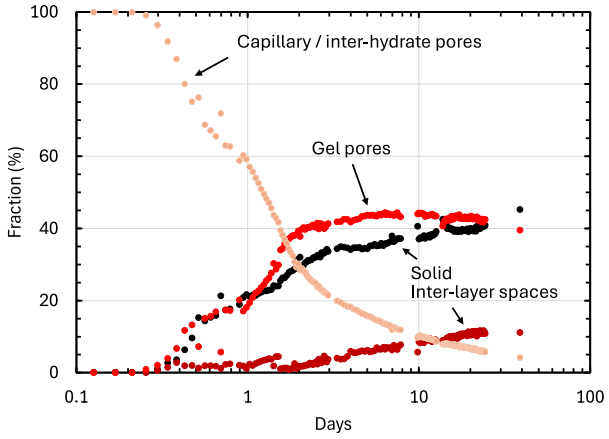

Fig. 8. Water fractions as a function of hydration time from spin-lock $T_{1\rho}$. Data are shown in progressively lighter shades for quasi-crystalline solid, inter-layer spaces, gel porosity and combined inter-hydrate and capillary porosity.

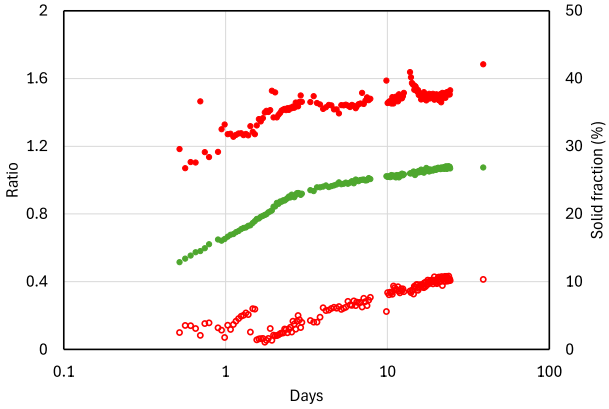

Fig. 9. The green symbols (right axis) show the quasi crystalline solid fraction as measured by solid echo against hydration time. The solid red symbols (left axis) show the solid signal enhancement factor when measured by spin-lock $T_{1\rho}$. The open red symbols are the spin-lock inter-layer fraction relative to the solid echo. (For interpretation of the references to colour in this figure legend, the reader is referred to the web version of this article.)

Fig. 9 shows the solid enhancement factor as a function of hydration time compared to the quadrature echo measurement which we regard as the "gold-standard" NMR measurement of the quasi-crystalline fraction. It is consistently greater than *c.* 1.0. Also shown is the spin-lock $T_{1\rho}$ inter-layer signal as a fraction of the quadrature echo solid signal. For CPMG, this would also be 'about 1.0' (Fig. 5), but is here much less.

6. Discussion

As just stated, the overall conclusion is that the partitioning of the water into solid hydrates and pores of different size as measured by spin-lock $T_{1\rho}$ is at first sight broadly in line with earlier results by CPMG but actually different in a very specific way. The $T_{1\rho}$ inter-layer signal is significantly diminished compared to CPMG and the solid signal correspondingly enhanced. A similar, but smaller effect is seen with the gel signal.

In order to interpret the diminution of the inter-layer mobile signal we looked first for explanation in terms of systematic error. Conceivably the experiment is sensitive to the homogeneity of the P^{90} pulse and the accuracy of the phase shift of the spin-lock pulse. On modern spectrometers, the radio frequency signal is digitally generated using a master clock/oscillator and so we have little reason to doubt the phase. Indeed, by deliberately offsetting the phase we produced a strong amplitude modulation of the signal as is to be expected from NMR theory. The initial P^{90} is, of necessity, spatially inhomogeneous across the sample. However by reducing the sample size, that inhomogeneity is reduced in absolute terms. We repeated the experiment using a sample of *circa* 1/3 size in all dimensions (1/27 volume). Apart from reducing the signal to noise ratio per unit measurement time, this had no effect: the inter-layer signal diminution remained. We are therefore left to conclude that the effect is real.

Before proceeding to discuss possible cement science reasons for this effect, we recap the underlying hypothesis of ^{1}H NMR porosimetry encapsulated in the so-called, and generally very well establish, fast-exchange model of relaxation [38–40]. Water associated with a pore surface has limited mobility and may be in close association with paramagnetic ions incorporated into the surface. As a result it has a short relaxation time, typically a few microseconds, comparable to solids. On the other hand, water molecules in the bulk pore fluid are mobile and have a long relaxation time, typically many milliseconds. Surface and bulk hydrogen are generally in fast exchange. Therefore the observed relaxation rate is the weighted average for hydrogen in the two site types. It is a measure of the surface to volume ratio. In this way, the relaxation time is a measure of pore size and the associated signal intensity is a measure of the total volume of water in all pores of that size.

According to the new experiments, seemingly there is a ^{1}H/water population in cement paste which appears to be in pore spaces, that is 'mobile-like', in a CPMG experiment and correspondingly does not appear 'solid-like' in a quadrature-echo experiment but which does not appear 'mobile-like' in a spin-lock $T_{1\rho}$ experiment and by default is therefore 'solid-like'. How might this be reconciled? We consider three possible explanations based around sub-partitioning of water incorporated in (i) ettringite, (ii) calcium hydroxide and (iii) inter-layer spaces.

The ^{1}H NMR characteristics of water populations in bulk samples of ettringite are relatively poorly defined and might offer a potential explanation except that the amount of ettringite in a low C_3A cement is surely too small to produce an effect in magnitude equivalent to about $\frac{1}{2}$ of the total quasi-crystalline (mainly $Ca(OH)_2$) fraction.

Equally, *bulk* samples of powdered $Ca(OH)_2$ are known to adsorb water and are usually oven dried before ^{1}H NMR analysis whereupon a modest (and highly variable) mobile water signal is removed. However, to the best of our knowledge, there has never been a suggestion that this is an issue for nanoscopic, quasi-crystalline $Ca(OH)_2$ in cement. Indeed, all our previous work looking at the density of C-S-H implicitly assumed it was not: the calcium hydroxide is $Ca(OH)_2$ with no spurious adsorbed water.

A more likely explanation is that the $T_{1\rho}$ experiment is partitioning inter-layer water in a different way to CPMG. If so, this is a very interesting result. We may have stumbled across something long wanted but elusive: a methodology to partition water *within* the smallest nano-spaces using ^{1}H NMR relaxation analysis.

We can simplistically divide C-S-H inter-layer ^{1}H into three sub-divisions as shown in the expanded section of Fig. 2: (i) ^{1}H in OH groups tightly bound to the hydrate backbone surfaces; (ii) ^{1}H in water strongly associated with Ca ions in the inter-layer space and (iii) ^{1}H in 'mobile' (evaporable) water neither associated with surfaces nor Ca ions.

The fact that a similar, but much smaller, effect is observed for gel water leads us to suspect surface OH hydrogen as the key fraction. The greater gel pore 'size' (by a factor of 3–5 as estimated by NMR) compared to inter-layer space and therefore the smaller fraction of 'surface' sites would be consistent with the difference in scale of the signal diminution. However, this is the entirety of our evidence for this assignment.

One difficulty with this analysis however is that, since the growth of quasi-crystalline solids broadly parallels that of the hydrate chains and gel porosity, then we would expect a more-or-less constant *ratio* of the different signal intensities across the course of hydration. At early ages in particular, where growth is fast, we did not see this, Fig. 9, red symbols. Does this observation have implications for understanding the way in which C-S-H grows at early age?

We finish with a second difficulty of this analysis. High field (normal) T_1 and T_2 relaxation times for bulk liquids such as water are normally the same. In small cement pores with relaxation mediated by paramagnetic impurities at surfaces, T_1 exceeds T_2 by a constant factor, typically 4 [3,7]. $T_{1\rho}$ is the low field equivalent of high field T_1. Experimentally here, with a very small B_{SL}, $T_{1\rho}$ and T_2 are found to be the same. They are expected to be controlled by molecular dynamics working on the same timescales and so this is not overly surprising. However, if they are the same, then the changed partitioning of water is difficult to understand. Why is (spin) exchange averaging sufficient to average the relaxation of the three ^{1}H sub-fractions in the inter-layer space in the CPMG (T_2) experiment but not the spin-lock $T_{1\rho}$ experiment? In order to better understand this, we are approaching the problem on three fronts. First, experimentally, the transition from low to high field becomes interesting as it evidences dynamics. This can be investigated using spin-lock $T_{1\rho}$ by measuring $T_{1\rho}$ as a function of the spin-lock pulse amplitude, B_{SL}. The frequency range covered is similar to the useful range of field-cycling experiments previously mentioned, but the spin-lock experiment is much easier and evidently more sensitive to different water populations. Moreover, it can be used throughout hydration, not just during the induction period. Second, molecular dynamics simulations of water in ultra-thin pores are being used to numerically calculate relaxation times. Third, the 3-tau model of relaxation in small pores [34] is being updated to include explicitly $T_{1\rho}$. The 3-tau model significantly updates and improves upon Korb's model of the frequency dependence of relaxation in small pores [33] yielding the full frequency (f) dependence of the relaxation times $T_1(f)$ and $T_2(f)$ in terms of 5 fit parameters. These are the surface water dynamics time constant, τ_l, derived from the surface water diffusion coefficient $D_s = \delta^2/(6\tau_l)$ where $\delta = 0.27$ nm; the surface desorption time constant τ_d; the bulk water time constant, τ_b derived from the bulk water diffusivity $D_b = \delta^2/(6\tau_b)$; the pore surface to volume ratio S/V; and the paramagnetic spin density of the solids, N_σ. Values of τ_l and τ_d normally lie in the range 0.1 to 10 μs in cement-based materials.

However these considerations evolve, it is evidently the case that spin-lock $T_{1\rho}$ is opening a new window on water dynamics in the very smallest nano-spaces of cement, a conundrum that has existed since inter-layer to gel-pore water exchange was first measured and found to be 'slow' in 2006 [8].

7. Conclusion

The experiments reported in this work have demonstrated the spin-lock $T_{1\rho}$ experiment as an alternative to combined CPMG and quadrature echo for measuring the partitioning of water between solid phases and pore spaces of different size in cement pastes. The experiment has the advantage of making it easier to analyse signal from water in small pores (inter-layer spaces) in particular. However, the experiments have also thrown up a result yet to be fully understood. The water in inter-layer spaces as measured by spin-lock and CPMG is resolved differently leading to the possibility that sub-populations of water in inter-layer spaces can be distinguished. Also, for the future, spin-lock experiments as a function of pulse power are expected to offer an experimentally easier route than ^{1}H field cycling to understanding the dynamics of water in pores.

CRediT authorship contribution statement

Peter J. McDonald: Writing – original draft, Methodology, Conceptualization. **David A. Faux:** Writing – review & editing. **Longfei Ma:** Investigation, Formal analysis, Data curation. **Hong Wong:** Writing – review & editing, Supervision, Resources.

Declaration of competing interest

The authors declare that they have no known competing financial interests or personal relationships that could have appeared to influence the work reported in this paper.

Data availability

Data will be made available on request.

References

[1] A.C.A. Muller, K.L. Scrivener, A.M. Gajewicz, P.J. McDonald, Densification of C–s–H measured by ^{1}H NMR relaxometry, J. Phys. Chem. C 117 (1) (2013) 403–412.

[2] A.C.A. Muller, K.L. Scrivener, A.M. Gajewicz, P.J. McDonald, Use of bench-top NMR to measure the density, composition and desorption isotherm of C–S–H in cement paste, Microporous Mesop. Mater. 178 (2013) 99–103.

[3] R. Blinc, M. Burgar, G. Lahajnar, M. Rozmarin, V. Rutar, I. Kocuvan, J. Ursic, NMR relaxation study of adsorbed water in cement and C_3S pastes, J. Am. Ceram. Soc. 61 (1–2) (1978) 35–37.

[4] J. Greener, H. Peemoeller, C. Choi, R. Holly, E.J. Reardon, C.M. Hansson, M.M. Pintar, Monitoring of hydration of white cement paste with proton NMR spin–spin relaxation, J. Am. Ceram. Soc. 83 (3) (2000) 623–627.

[5] A.M. Gajewicz-Jaromin, P.J. McDonald, A.C.A. Muller, K.L. Scrivener, Influence of curing temperature on cement paste microstructure measured by ^{1}H NMR relaxometry, Cem. Conc. Res. 122 (2019) 147–156.

[6] A.C.A. Muller, K.L. Scrivener, J. Skibsted, A.M. Gajewicz, P.J. McDonald, Influence of silica fume on the microstructure of cement pastes: New insights from ^{1}H NMR relaxometry, Cem. Conc. Res. 74 (2015) 116–125.

[7] P.J. McDonald, J.P. Korb, J. Mitchell, L. Monteilhet, Surface relaxation and chemical exchange in hydrating cement pastes: A two-dimensional NMR relaxation study, Phys. Rev. E 72 (1) (2005) 011409:1–9.

[8] L. Monteilhet, J.P. Korb, J. Mitchell, P.J. McDonald, Observation of exchange of micropore water in cement pastes by two-dimensional T_2-T_2 nuclear magnetic resonance relaxometry, Phys. Rev. E 74 (6) (2006) 061404:1–9.

[9] M. Wyrzykowski, P.J. McDonald, K.L. Scrivener, P. Lura, Water redistribution within the microstructure of cementitious materials due to temperature changes studied with ^{1}H NMR, J. Phys. Chem. C 121 (50) (2017) 27950–27962.

[10] M. Wyrzykowski, A.M. Gajewicz-Jaromin, P.J. McDonald, D.J. Dunstan, K.L. Scrivener, P. Lura, Water redistribution-microdiffusion in cement paste under mechanical loading evidenced by ^{1}H NMR, J. Phys. Chem. C 123 (26) (2019) 16153–16163.

[11] N. Fischer, R. Haerdtl, P.J. McDonald, Observation of the redistribution of nanoscale water filled porosity in cement based materials during wetting, Cem. Conc. Res. 68 (2015) 148–155.

[12] A.M. Gajewicz, E. Gartner, K. Kang, P.J. McDonald, V. Yermakou, A ^{1}H NMR relaxometry investigation of gel-pore drying shrinkage in cement pastes, Cem. Conc. Res. 86 (2016) 12–19.

[13] P.J. McDonald, O. Istok, M. Janota, A.M. Gajewicz-Jaromin, D.A. Faux, Sorption, anomalous water transport and dynamic porosity in cement paste: A spatially localised ^{1}H NMR relaxation study and a proposed mechanism, Cem. Conc. Res. 133 (2020) 1–12.

[14] M. Janota, O. Istok, D.A. Faux, P.J. McDonald, Factors influencing the time dependence of porosity relaxation in cement during sorption: Experimental results from spatially resolved NMR, Cement 8 (2022) 100028:1–14.

[15] M. Zalzale, P.J. McDonald, Lattice Boltzmann simulations of the permeability and capillary adsorption of cement model microstructures, Cem. Conc. Res. 42 (12) (2012) 1601–1610.

[16] P.J. McDonald, M.N. Borg, D.A. Faux, Mesoscale modelling of dynamic porosity in cement hydrate gel during a water sorption cycle: A lattice Boltzmann study, Cem. Conc. Res. 146 (2021) 106475:1–17.

[17] M.A. Etzold, P.J. McDonald, A.F. Routh, Growth of sheets in 3D confinements - a model for the C–S–H meso structure, Cem. Conc. Res. 63 (2014) 137–142.

[18] D.A. Faux, P.J. McDonald, Nuclear-magnetic-resonance relaxation rates for fluid confined to closed, channel, or planar pores, Phys. Rev. E 98 (6) (2018) 063110:1–14.

[19] D. Faux, R. Kogon, V. Bortolotti, P. McDonald, Advances in the interpretation of frequency-dependent nuclear magnetic resonance measurements from porous material, Molecules 24 (20) (2019) 3688:1–13.

[20] A. Valori, P.J. McDonald, K. Scrivener, The morphology of C–S–H: Lessons from ^{1}H nuclear magnetic resonance relaxometry, Cem. Conc. Res. 49 (2013) 65–81.

[21] S.M. Nagel, C. Strangfeld, S. Kruschwitz, Application of ^{1}H proton NMR relaxometry to building materials – A review, J. Magn. Reson. Open 6–7 (2021) 100012.

[22] A.C.A. Muller, J. Mitchell, P.J. McDonald, Proton nuclear magnetic resonance relaxometry, in: R. Snellings, K. Scrivener, B. Lothenbach (Eds.), A Practical Guide to Microstructural Analysis of Cementitious Materials, Taylor & Francis Group, United Kingdom, 2015.

[23] P.J. McDonald, A.M. Gajewicz-Jaromin, R. Morrell, The Characterisation of Cement Based Materials Using T_2 ^{1}H Nuclear Magnetic Resonance Relaxation Analysis, Report 44, National Physical Laboratory, UK, 2017, pp. 1–165.

[24] A.G. Anderson, S.R. Hartmann, Nuclear magnetic resonance in the demagnetized state, Phys. Rev. 128 (5) (1962) 2023–2041.

[25] M. Fleury, F. Deflandre, Quantitative evaluation of porous media wettability using NMR relaxometry, Magn. Reson. Imaging 21 (3–4) (2003) 385–387.

[26] K. Tolkkinen, O. Mankinen, S.E. Mailhiot, V.-V. Telkki, Ultrafast T_1-$T_{1\rho}$ NMR for correlating different motional regimes of molecules, Anal. Chem. 96 (2024) 16534–16542.

[27] S. Meiboom, D. Gill, Modified spin echo method for measuring nuclear relaxation times, Rev. Sci. Instrum. 29 (1958) 688–691.

[28] J.G. Powles, J.H. Strange, Zero time resolution nuclear magnetic resonance transient in solids, Proc. Phys. Soc. 82 (1) (1963) 6–15.

[29] P.J. McDonald, B. Newling, Stray field magnetic resonance imaging, Rep. Progr. Phys. 61 (11) (1998) 1441–1493.

[30] E.L. Hahn, An accurate nuclear magnetic resonance method for measuring spin-lattice relaxation times, Phys. Rev. 76 (1) (1949) 145–146.

[31] M. Pang, Z. Sun, Q. Li, J. Yanliang, ^{1}H NMR spin-lattice relaxometry of cement pastes with polycarboxylate superplasticizers, Materials 13 (2020) 5626.

[32] A. Plassais, M.P. Pomiès, N. Lequeux, P. Boch, J.P. Korb, D. Petit, F. Barberon, Micropore size analysis by NMR in hydrated cement, Magn. Reson. Imaging 21 (3–4) (2003) 369–371.

[33] F. Barberon, J.P. Korb, D. Petit, V. Morin, E. Bermejo, Probing the surface area of a cement-based material by nuclear magnetic relaxation dispersion, Phys. Rev. Lett. 90 (11) (2003) 116103.

[34] D.A. Faux, P.J. McDonald, A model for the interpretation of nuclear magnetic resonance spin-lattice dispersion measurements on mortar, plaster paste, synthetic clay and oil-bearing shale, Microporous Mesop. Mater. 269 (2018) 39–42.

[35] R. Kogon, D. Faux, 3TM: Software for the 3-Tau model, SoftwareX 17 (2022) 100979:1–9.

[36] D.A. Faux, O. Istok, A.A. Rahaman, P.J. McDonald, E. McKiernan, D.F. Brougham, Nuclear spin relaxation in aqueous paramagnetic ion solutions, Phys. Rev. E 107 (5) (2023) 054605:1–21.

[37] M.M. Rusu, D. Faux, I. Ardelean, Monitoring the effect of calcium nitrate on the induction period of cement hydration via low-field NMR relaxometry, Molecules 28 (2) (2023) 476:1–12.

[38] J.R. Zimmerman, W.E. Brittin, Nuclear magnetic resonance studies in multiple phase systems: Lifetime of a water molecule in an adsorbing phase on silica gel, J. Phys. Chem. 61 (10) (1957) 1328–1333.

[39] K. Brownstein, C. Tarr, Spin-lattice relaxation in a system governed by diffusion, J. Magn. Reson. (1969) 26 (1) (1977) 17–24.

[40] F. D'Orazio, J. Tarczon, W.P. Halperin, K. Eguchi, T. Mizusaki, Application of nuclear magnetic resonance pore structure analysis to porous silica glass, J. Appl. Phys. 65 (2) (1989) 742–751.